



# MICAS: Multi-grained In-Context Adaptive Sampling for 3D Point Cloud Processing

Feifei Shao<sup>1</sup>, Ping Liu<sup>2</sup>, Zhao Wang<sup>1</sup>, Yawei Luo<sup>1,\*</sup>, Hongwei Wang<sup>1</sup>, Jun Xiao<sup>1</sup>

<sup>1</sup>Zhejiang University, China <sup>2</sup> University of Nevada, Reno, USA

{sff, zhao.wang, yaweiluo}@zju.edu.cn, pino.pingliu@gmail.com,  
hongweiwang@intl.zju.edu.cn, junx@cs.zju.edu.cn

## Abstract

*Point cloud processing (PCP) encompasses tasks like reconstruction, denoising, registration, and segmentation, each often requiring specialized models to address unique task characteristics. While in-context learning (ICL) has shown promise across tasks by using a single model with task-specific demonstration prompts, its application to PCP reveals significant limitations. We identify inter-task and intra-task sensitivity issues in current ICL methods for PCP, which we attribute to inflexible sampling strategies lacking context adaptation at the point and prompt levels. To address these challenges, we propose MICAS, an advanced ICL framework featuring a multi-grained adaptive sampling mechanism tailored for PCP. MICAS introduces two core components: task-adaptive point sampling, which leverages inter-task cues for point-level sampling, and query-specific prompt sampling, which selects optimal prompts per query to mitigate intra-task sensitivity. To our knowledge, this is the first approach to introduce adaptive sampling tailored to the unique requirements of point clouds within an ICL framework. Extensive experiments show that MICAS not only efficiently handles various PCP tasks but also significantly outperforms existing methods. Notably, it achieves a remarkable 4.1% improvement in the part segmentation task and delivers consistent gains across various PCP applications.*

## 1. Introduction

Deep learning has greatly advanced 3D point cloud processing, tackling tasks like semantic segmentation [24, 49], registration [64, 73], reconstruction [18, 37], and denoising [34, 57]. However, achieving high performance often requires separate models for each task, increasing complexity and resource demands. Multi-task Learning (MTL) [48, 72, 75] attempts to reduce this burden by training models to

handle multiple tasks simultaneously, but it struggles with performance trade-offs and complex parameter tuning. In contrast, In-context Learning (ICL) [11, 22, 62] offers a simpler approach, using only a few prompts to guide a single model in performing multiple tasks without changing its parameters [1, 3, 35, 54, 55, 62].

Despite these advancements, recent efforts to extend ICL to 3D point cloud processing [11, 31] reveal significant limitations. Specifically, these studies have not fully addressed critical challenges associated with conventional point cloud sampling techniques used in the ICL framework. Taking Figure 1 (a) for example, the ICL framework manages multiple point cloud tasks, each with distinct preferences for point cloud sampling. However, conventional sampling methods struggle to adapt equally well to these diverse tasks simultaneously. These gaps, particularly in adapting sampling techniques to task-specific and prompt-specific contexts, hinder overall performance and reliability.

To overcome these limitations, our work tackles two critical issues: **1) Inter-task Sensitivity:** As illustrated in Figure 1 (b), task-agnostic sampling strategies, *e.g.*, Farthest Point Sampling (FPS), may perform differently across *different tasks*, such as reconstruction and denoising. This difference arises because FPS tends to prioritize outliers, often leading to the selection of noisy points. This issue underscores the urgent need for a methodology that effectively integrates task information into the sampling process. **2) Intra-task Sensitivity:** Depicted in Figure 1 (c), variations in prompts for the *same task* can yield divergent sampling outcomes, resulting in inconsistent experimental results. This highlights the need to replace generic prompts with carefully curated, query-specific prompts.

To effectively address the inter-task and intra-task sensitivity issues, we introduce a novel Multi-grained In-Context Adaptive Sampling mechanism, dubbed MICAS, for 3D point cloud in-context learning. As shown in Figure 2 (b), MICAS comprises two integral components: task-adaptive point sampling and query-specific prompt sampling.

\*Yawei Luo is the corresponding author.

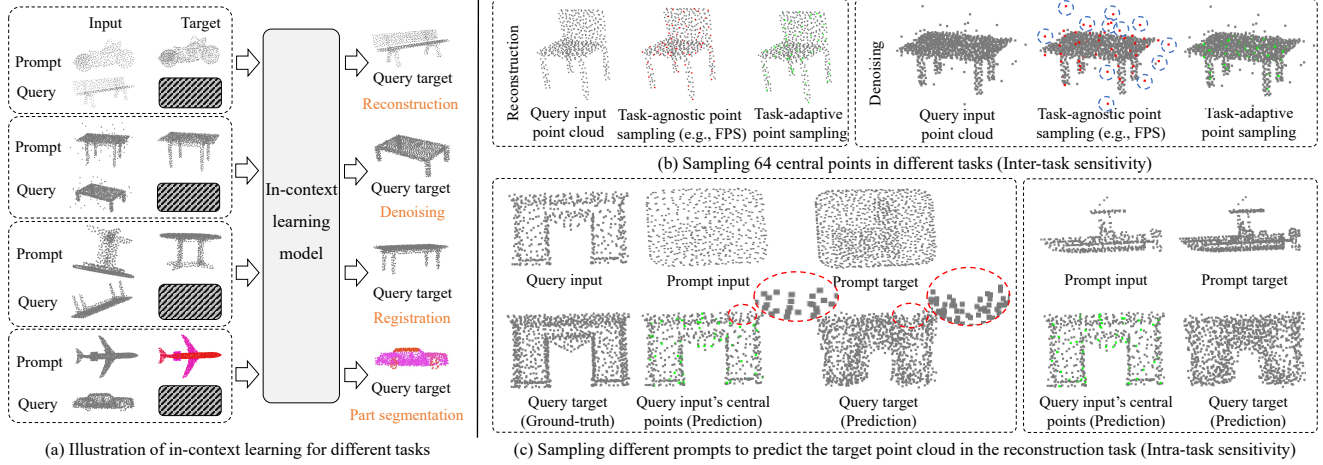


Figure 1. Inter-task and intra-task sensitivities in in-context learning. The red and green points are sampled using Farthest Point Sampling (FPS) and task-adaptive point sampling, respectively. The blue circles indicate erroneous sampling points, while the red ovals highlight missing points in the predicted point cloud, caused by the absence of a central point within the region. (Zoom in for more details)

For inter-task sensitivity, task-adaptive point sampling enables adaptive sampling by interpreting various prompts, operating in two stages: prompt understanding and Gumbel sampling. First, the prompt understanding phase extracts essential task features from the prompt and corresponding point features from point clouds, providing a basis for informed sampling. However, traditional discrete sampling methods fail to support gradient-based optimization, jeopardizing both the efficiency and effectiveness of the learning process. To address this, the Gumbel sampling phase leverages the Gumbel-softmax [19], transforming discrete sampling into a differentiable operation and enabling a fully learnable and efficient sampling process [58].

To mitigate the intra-task sensitivity caused by prompt variability, we integrate a query-specific prompt sampling module. This module selects the most effective prompt by ranking the sampling probabilities, which are aligned to the inference performance. Specifically, we first predict sampling probabilities for each prompt by analyzing queries and prompts, followed by aligning these probabilities with the in-context learning model’s performance. During inference, the “best-performing” prompt is selected based on these probabilities among strategically chosen candidate prompts.

We evaluate our design on a benchmark [11] comprising multiple existing datasets [5, 66], covering four distinct point cloud tasks with five levels of difficulty each. Our comprehensive evaluation demonstrates the efficacy of MICAS in addressing both inter-task and intra-task sensitivity issues. In addition, these results highlight the practical advantages of MICAS, including enhanced adaptability to diverse 3D point cloud tasks and improved robustness across various ICL model variants. The contributions of this paper are summarized as follows:

- We propose a novel multi-grained in-context adap-

tive sampling mechanism, MICAS, that effectively addresses inter-task and intra-task sensitivity issues in 3D point cloud in-context learning.

- MICAS integrates two key components: task-adaptive point sampling and query-specific prompt sampling. The former dynamically adjusts to task-specific needs at the point level, while the latter refines prompt selection to minimize intra-task variability. Together, these components enable adaptive and efficient sampling across diverse 3D point cloud tasks.
- Extensive experiments demonstrate that MICAS not only simplifies training and efficiently handles multiple tasks but also achieves substantial performance gains over previous state-of-the-art methods, including a notable 4.1% increase in the part segmentation task.

## 2. Related Work

### 2.1. Sampling Methods for Point Cloud

Point cloud sampling is essential for representing object shape and topology efficiently, enabling large-scale point cloud analysis [29, 32, 36, 58]. Existing methods can be categorized into mathematical statistics-based and learnable task-based approaches. First, mathematical statistics-based methods [6, 13, 17, 29, 44, 51] are task-agnostic, leveraging structural and geometric properties. Techniques include random sampling [17], grid sampling [51], farthest point sampling (FPS) [29, 44], and Inverse Density Importance Sampling (IDIS) [13]. While effective, these methods overlook task-specific information. Second, learnable task-based methods [9, 26, 58, 63] design sampling networks tailored to specific tasks and guided by task losses. Dovrat *et al.* [9] propose S-Net, a learnable network that generates point subsets and enhances them with ProgressiveNet,

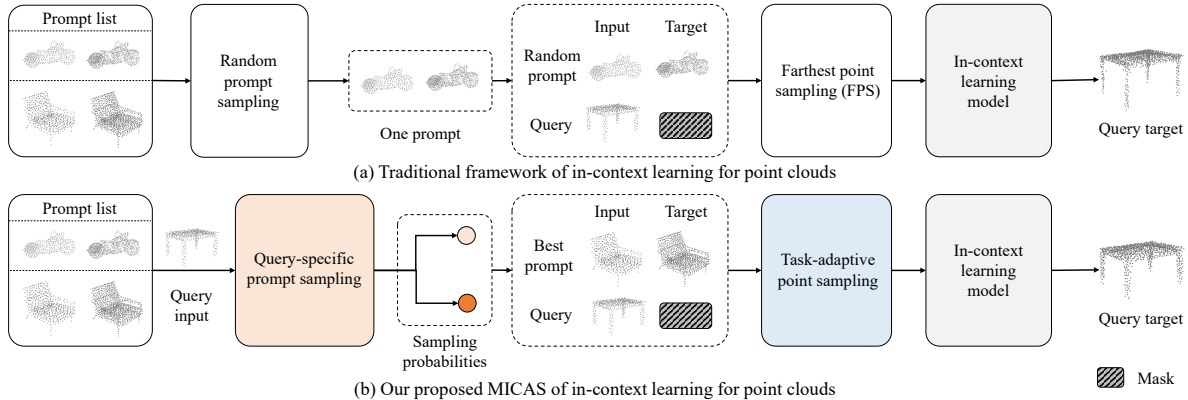


Figure 2. Comparison between the proposed MICAS and the traditional in-context learning framework.

which prioritizes task-relevant points. SampleNet [26] introduces differentiable sampling using weighted averages of nearest neighbors, while IndexSample [60] improves results with a confidence layer. SkeletonNet [58] uses Gumbel-softmax for discrete sampling, and CP-Net [39] performs adaptive down-sampling. PAT [65] employs group shuffle attention, PointASNL [63] adaptively adjusts point features and local normalization, Pra-net [7] integrates intra-region structure learning for local adaptation, and APES [59] utilizes edge detection for adaptive sampling.

However, existing mathematical statistics-based sampling overlooks information from both the point cloud and the task. Meanwhile, existing learnable task-based sampling focuses on inter-point cloud adaptation within the same task, neglecting inter-task adaptation within the same point cloud. To handle this issue, we propose task-adaptive point sampling to leverage task-specific information from prompts for customized, efficient sampling across tasks.

## 2.2. Demonstration Retrieval for ICL

The sensitivity of in-context learning to demonstration selection [62] has led to the development of various retrieval techniques, categorized into similarity-based and diversity-based methods. First, similarity-based retrieval assumes that demonstrations resembling the query provide valuable guidance [30]. Methods like KATE [30] retrieve semantically similar examples to construct prompts, while EPR [47] uses similarity scores based on inner products. PARC [41] enriches contexts with semantically similar sentences, and UDR [28] introduces a multi-task list-wise ranking framework to mine high-quality demonstrations. Second, diversity-based retrieval focuses on reducing redundancy, providing varied perspectives, and ensuring query coverage [27, 67, 74]. Auto-CoT [74] diversifies sampled questions to construct reasoning chains, GENREAD [67] uses clustering to synthesize prompts from diverse clusters, and Cover-LS [27] selects demonstrations that ensure structural coverage for better generalization.

Drawing inspiration from existing demonstration retrieval methods, we implement a simple yet effective probability-based retrieval approach of 3D point cloud, introducing a novel query-specific prompt sampling module.

## 2.3. Point Cloud in Large Language Model Era

With the rapid advancements in Large Language Models (LLMs)[46, 52], various point cloud methods integrating LLMs have emerged. For example, PointCLIP[70] and CLIP2 [69] align 3D data with language representations, leveraging multi-view depth maps and few-shot fine-tuning, triplet proxies collection scheme and cross-modal pretraining, respectively. MiniGPT-3D [50] efficiently aligns 3D data with LLMs using 2D priors. Point-E [40] generates 3D point clouds from prompts, and PointBind [15] offers a unified framework for 3D multi-modal tasks. PointLLM [61] and SegPoint [16] utilize LLaMA [52] for understanding point clouds, while PIC [11] and DG-PIC [22] apply ICL for multi-task and multi-domain point cloud processing.

In this work, we find the inter-task and intra-task sensitivity issues in current ICL methods of point clouds, stemming from inflexible sampling strategies that lack context adaptation at both the point and prompt levels. To address these challenges, we propose an enhanced ICL method with a multi-grained adaptive sampling mechanism.

## 3. Methodology

### 3.1. Preliminaries

**Problem Settings.** We formally define the problem settings for in-context learning with 3D point clouds. As illustrated in Figure 2 (a), each input sample comprises two pairs of “input-target” point clouds, similar to the setup used in 2D-context learning [11]. One pair serves as a prompt, and the other pair serves as a query. Each pair consists of an input point cloud and its corresponding output point cloud for the given task [11, 62]. The prompts represent four typical PCP tasks: reconstruction [21, 37], denoising [20, 34],

registration [43, 64], and part segmentation [25, 49]. Following established protocols [11, 31], the network is trained to reconstruct randomly masked parts of the “target” point cloud in both the prompt and the query. During inference, the model reconstructs the “target” point cloud of the query.

**Revisiting Point Cloud In-Context Learning Model.** Before presenting our method, we formally introduce the framework of in-context learning for point clouds. Using the pioneering work PIC [11] as an example, which introduces a new benchmark, the framework comprises data processing, model design, and model training.

Regarding data processing, PIC [11] begins by considering two pairs of “input-target” point clouds, denoted as query  $Q = (X_q, Y_q)$  and prompt  $P = (X_p, Y_p)$ . It first applies Farthest Point Sampling (FPS) [44] to select  $N$  central points  $C_{X_q}$  and  $C_{X_p}$  from  $X_q$  and  $X_p$ , respectively. To ensure alignment between the sampled central points derived from the “input” and “target” point clouds, a Joint Sampling (JS) module is employed. This module uses the point indexes of central points  $C_{X_q}$  and  $C_{X_p}$  to locate the corresponding position points in the “target” point clouds  $Y_q$  and  $Y_p$  as their center points  $C_{Y_q}$  and  $C_{Y_p}$ , respectively. Subsequently, the K-Nearest Neighbors (KNN)[12] technique transforms  $(X_q, Y_q, X_p, Y_p)$  into  $N$  point patches  $(R_{X_q}, R_{Y_q}, R_{X_p}, R_{Y_p})$  based on these central points, which are then encoded into tokens. Finally, these point patches are encoded into tokens.

In model design, PIC [11] adopts a mask-point modeling (MPM) strategy with a transformer-based encoder-decoder architecture. A  $1 \times 1$  convolutional layer serves as the task head for reconstructing the point clouds.

During model training, PIC [11] utilizes two pairs of point patches, the query point patches  $(R_{X_q}, R_{Y_q})$  and the prompt point patches  $(R_{X_p}, R_{Y_p})$ , to perform a masked point reconstruction task. It first randomly masks the point patches within  $R_{Y_q}$  and  $R_{Y_p}$  and then trains the model using the Chamfer Distance [10] loss  $\mathcal{L}_{cd}$ , defined as:

$$\begin{aligned} \mathcal{L}_{cd}(R_{pred}, G) = & \frac{1}{|R_{pred}|} \sum_{r \in R_{pred}} \min_{g \in G} \|r - g\|_2^2 \\ & + \frac{1}{|G|} \sum_{g \in G} \min_{r \in R_{pred}} \|g - r\|_2^2, \end{aligned} \quad (1)$$

where  $\mathcal{L}_{cd}$  measures the discrepancy between each predicted patch  $R_{pred}$  and its corresponding ground truth patch  $G$ ,  $|R_{pred}|$  and  $|G|$  represent the number of points in patch  $R_{pred}$  and patch  $G$ , respectively. During inference, the model predicts the entire masked “target” point cloud  $Y_q$  for the query, which is shown in Figure 2 (a).

However, PIC [11] employs Farthest Point Sampling (FPS), which lacks context adaptation at both the point and prompt levels, leading to sensitivity issues across and within tasks. As shown in Figure 1 and Table 2, FPS often se-

lects noisy points as center points in the denoising task, causing the model’s CD loss to remain high. To overcome these critical limitations, we propose a novel Multi-grained In-Context Adaptive Sampling mechanism, dubbed MICAS, which fundamentally rethinks point cloud in-context learning by incorporating task-adaptive point sampling and query-specific prompt sampling. This new approach significantly enhances the adaptability and robustness of point cloud processing tasks shown in Figure 4 and Table 2, addressing the inter-task and intra-task sensitivity issues that previous methods, such as PIC, fail to resolve.

### 3.2. Task-adaptive Point Sampling

As illustrated in Figure 3 (b), we introduce a task-adaptive point sampling module to address the *inter-task sensitivity* (cf. Figure 1 (a)) by focusing on understanding and applying task information from prompts during the sampling stage. This module comprises two key components: prompt understanding, which extracts relevant task features and point features, and Gumbel sampling, which achieves differentiable sampling via the Gumbel-softmax [19, 65] leveraging these extracted dual-level features.

**1) Prompt Understanding.** To accurately understand the point cloud information in the “input-target” point clouds of query  $Q = (X_q, Y_q)$  and prompt  $P = (X_p, Y_p)$ , we adopt PointNet [43] as our task encoder and point encoder, as shown in Figure 3 (a). First, we employ a task encoder that incorporates the max pooling layer and previous from the PointNet classification branch [43], enabling it to extract task-relevant information from prompts. Its objective is to process the prompt  $P = (X_p, Y_p)$  and generate the corresponding task feature  $F_{task}$ . Specifically, we concatenate the prompt  $P = (X_p, Y_p)$ , and feed this concatenation into the task encoder  $\Phi_{task}$  to yield the task feature  $F_{task}$ :

$$F_{task} = \Phi_{task}(X_p \oplus Y_p), \quad (2)$$

where  $\oplus$  denotes concatenation operation.

Second, to extract point feature information from each point cloud, we employ a point encoder based on the PointNet segmentation branch [43]. Its purpose is to process any given point cloud  $X_*$  and produce the associated point features  $F_{X_*}$ :

$$F_{X_*} = \Phi_{point}(X_*), \quad (3)$$

where  $X_*$  refers to any of the point clouds  $X_q, Y_q, X_p$ , and  $Y_p$ . Accordingly,  $F_{X_*}$  represents the features of point clouds, namely  $F_{X_q}, F_{Y_q}, F_{X_p}$ , and  $F_{Y_p}$ , respectively.

**2) Gumbel Sampling.** We utilize the task feature  $F_{task}$  and the point features  $F_{X_q}$  and  $F_{X_p}$  to achieve differentiable sampling by integrating the Gumbel-softmax approach [19, 65]. This method performs a “soft” selection that mimics one-hot encoding by blending probabilities rather than making a hard selection of a single point.

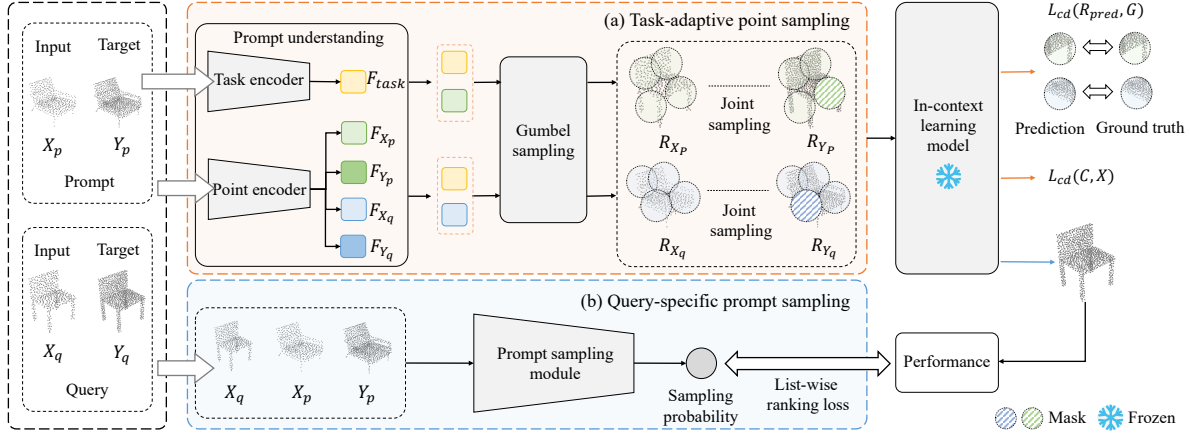


Figure 3. Overview of the proposed MAL-ICL. (a) Task-adaptive point sampling is designed to achieve better point-level sampling. (b) Query-specific prompt sampling aims to infer the most effective prompt-level sampling.

As illustrated in Figure 3 (a), we initially merge the task feature  $F_{task} \in \mathbb{R}^{d1}$  with the point feature  $F_{X_q} \in \mathbb{R}^{S \times d2}$  to create enhanced point features  $\hat{F}_{X_q} \in \mathbb{R}^{S \times (d1+d2)}$ :

$$\hat{F}_{X_q} = F_{task} \oplus F_{X_q}, \quad (4)$$

where  $d1$  and  $d2$  represent the feature dimensions, and  $S$  denotes the number of points in the point cloud. Then, the enhanced point features  $\hat{F}_{X_q}$  are passed through a fully connected layer with weight parameter  $W \in \mathbb{R}^{(d1+d2) \times N}$  to yield sampling weights  $SW \in \mathbb{R}^{S \times N}$ :

$$SW = \hat{F}_{X_q} \times W, \quad (5)$$

where  $N$  indicates the number of selected points.

Subsequently, the sampling weight  $SW$  is normalized using the Gumbel-softmax [19, 65], which employs a discrete reparameterization technique to obtain smooth gradients by continuously relaxing the categorical variable [58]. Given the Gumbel noise  $g = (g_1, \dots, g_k)$ , where each  $g_i$  is independently drawn from a Gumbel distribution within 0 and 1, the soft sampling weight  $SW_{gs}$  is calculated as:

$$SW_{gs} = \text{softmax}((\log(SW) + g)/\tau), \quad (6)$$

where  $\tau > 0$  is the annealing temperature, and the softmax function operates along the dimension of points. The Gumbel-softmax mechanism ensures that the newly generated points remain within the three-dimensional space of the original point cloud. Ultimately, the selected central points  $C_{X_q} \in \mathbb{R}^{N \times 3}$  are generated by projecting the sampling weight  $SW_{gs}$  onto the original point cloud  $X_q \in \mathbb{R}^{S \times 3}$ :

$$C_{X_q} = SW_{gs}^T \times X_q. \quad (7)$$

The same process is applied to derive the sampling points  $C_{X_p}$  for the point cloud  $X_p$ . Following the methodology of Fang *et al.* [11], we employ Joint Sampling and KNN techniques to produce  $N$  point patches  $(R_{X_q}, R_{Y_q}, R_{X_p}, R_{Y_p})$ ,

which are then input into the in-context learning model (*e.g.*, PIC [11]) for masked point modeling.

**3) Loss Function.** To enhance the training of the task-adaptive point sampling module, we implement an additional  $\mathcal{L}_{cd}(C, X)$  loss function based on Equation 1. This new loss function quantifies the discrepancy between the sampled central points  $C$  and the original point cloud  $X$ , as shown in Figure 3. Finally, the training loss of the task-adaptive point sampling module, denoted as  $\mathcal{L}_{sampling}$ , is defined as follows:

$$\mathcal{L}_{sampling} = \mathcal{L}_{cd}(R_{pred}, G) + \alpha \cdot \mathcal{L}_{cd}(C, X), \quad (8)$$

where  $R_{pred}$  and  $G$  respectively represent the predicted patch and its ground-truth patch, as introduced in Equation 1. The hyperparameter  $\alpha$  is to modulate the influence of the CD loss between the sampled points and the original point cloud.

### 3.3. Query-specific Prompt Sampling

To address the *intra-task sensitivity* issue depicted in Figure 1 (c), we introduce a query-specific prompt sampling module designed to select the most suitable prompt, as depicted in Figure 3 (b).

**1) Pseudo Label.** Inspired by UDR [28], which addresses prompt retrieval in natural language processing, we collect training examples for our prompt sampling module by utilizing the output signals from the in-context learning model  $\Phi_{ICL}$  (*e.g.*, PIC [11]). Specifically, given a query “input” point cloud  $X_q$  and a prompt  $P = (X_p, Y_p)$ ,  $\Phi_{ICL}$  processes these inputs to generate a predicted query “target” point cloud  $\hat{Y}_q$ . We then evaluate the performance by comparing  $\hat{Y}_q$  with the ground-truth query “target” point cloud  $Y_q$ , using metrics such as CD loss or mIOU. The resulting performance serves as the pseudo label  $\tilde{y}$  for the training of the prompt sampling module, as illustrated in Figure 3:

$$\tilde{y} = \Phi_{ICL}(X_q, X_p, Y_p). \quad (9)$$

To ensure consistency across different tasks, we employ max-min normalization [23, 53]. This normalization maintains the maximum and minimum performance values for each task, allowing us to normalize performance indicators across different tasks to the range  $[0, 1]$ .

**2) Sampling Probability.** Our goal is to utilize the query “input” point cloud to generate a sampling probability for each candidate prompt. Specifically, we first combine the query “input” point cloud  $X_q$  with the prompt  $P = (X_p, Y_p)$  to form a fused point cloud  $\tilde{X} \in \mathbb{R}^{3 \times S \times 3}$ :

$$\tilde{X} = (X_q \oplus X_p \oplus Y_p), \quad (10)$$

where  $\oplus$  denotes the concatenation along the point dimension, and  $S$  represents the number of points in the point cloud. We randomly select  $K$  prompts for each query “input” point cloud, generating  $K$  new point clouds  $\tilde{X}_i$ . These  $\tilde{X}_i$  are then passed through the prompt sampling module  $\Phi_{prompt}$ <sup>1</sup> to produce  $K$  sampling probabilities  $Prob = \{prob_1, prob_2, \dots, prob_K\}$ , where each  $prob_i$  is defined as:

$$prob_i = \Phi_{prompt}(\tilde{X}_i). \quad (11)$$

**3) Loss Function.** Given a query “input” point cloud and  $K$  randomly selected prompts, we first generate  $K$  pseudo labels  $\tilde{Y} = \{\tilde{y}_1, \tilde{y}_2, \dots, \tilde{y}_K\}$  using Equation 9. Then, we compute  $K$  sampling probabilities  $Prob = \{prob_1, prob_2, \dots, prob_K\}$  by employing Equation 11. Finally, we utilize the list-wise ranking loss  $\mathcal{L}_{listwise\_rank}$  to evaluate and optimize ranking orders [4, 28, 62], as shown in Figure 3 (b).

$$\mathcal{L}_{listwise\_rank} = \sum_{i,j} \max\left(0, \frac{1}{r(\tilde{y}_i)} - \frac{1}{r(\tilde{y}_j)}\right) \times \log(1 + e^{(prob_j - prob_i)}), \quad (12)$$

where  $r(\tilde{y})$  indicates the ranking order of  $\tilde{y}$  among these candidate prompts.

During inference, given a query “input”  $X_q$ , we first use the prompt sampling module to select the best prompt with the highest probability among  $K$  candidates, as shown in Figure 2 (b). Then, we input  $X_q$  and selected prompt into PIC [11] to predict the “target” point cloud for the query.

### 3.4. Model Training

Task-adaptive point sampling learns each prompt individually, whereas query-specific prompt sampling evaluates multiple prompts simultaneously. Jointly training these two modules could increase the learning complexity of task-adaptive point sampling, slow convergence, and create unnecessary entanglement between the modules. Adopting a

<sup>1</sup>The prompt sampling module is model-agnostic. In this paper, we employ PointNet [43] as the prompt sampling module.

step-wise training strategy, as suggested in previous studies [2, 38], can simplify the problem, improve robustness, and make the learning process more manageable. Therefore, we employ this strategy for our proposed MICAS.

First, we train the task-adaptive point sampling module, replacing the central points typically selected by FPS with those produced by our sampling method. This phase focuses on optimizing point sampling and uses the Chamfer Distance (CD) loss (cf. Equation 8), while the query-specific prompt sampling module remains inactive.

Once the task-adaptive point sampling module is trained and its parameters are fixed, we proceed to train the query-specific prompt sampling module. This module analyzes each query and its candidate prompts to predict sampling probabilities, rank them, and optimize using the list-wise ranking loss (cf. Equation 12).

## 4. Experiments

### 4.1. Experimental Settings

**Dataset.** The proposed MICAS is rigorously evaluated using the ShapeNet In-Context Dataset, introduced in the PIC [11]. This dataset comprises “input-target” point cloud pairs, each derived from well-known repositories such as ShapeNet [5] and ShapeNetPart [66]. The “input” point cloud serves the task query, while the “target” represents the expected outcome. The dataset is extensive, featuring 174,404 samples for training and 43,050 for testing, across four distinct tasks: registration, reconstruction, denoising, and part segmentation. Each task is divided into five levels of difficulty to assess model performance comprehensively.

**Evaluation Metrics.** We employ the Chamfer Distance (CD) [10] and Mean Intersection over Union (mIOU) as the primary evaluation metrics for different tasks. For registration, reconstruction, and denoising tasks, CD is used to measure the structural discrepancy between the predicted and ground-truth point clouds. For part segmentation, mIOU is utilized to appraise segmentation performance.

**Implementation Details.** Following PIC [11], we sample 1,024 points from each point cloud and segment them into 64 patches, each containing 32 neighboring points. PointNet [43] is used as the task encoder, point encoder, and prompt sampling module (cf. Figure 3). For task-adaptive point sampling, we set the initial learning rate to 0.0001, reducing it to  $1e-6$  over 60 epochs using a Cosine Annealing Scheduler [33], with a batch size of 72 and a sampling loss hyperparameter  $\alpha$  of 0.5. For query-specific prompt sampling, 8 candidate prompts are randomly selected per query, with a learning rate of 0.00001, decay to 0.000001, 30 training epochs, and a batch size of 9.

**Model Variants.** PIC [11] includes two variants: PIC-Cat and PIC-Sep, which differ in how they combine “input” and “target” point clouds. PIC-Cat concatenates the “input” and

Table 1. Comparison with state-of-the-art models on the ShapeNet In-Context [11]. For reconstruction, denoising, and registration, we report Chamfer Distance (CD) [10] loss (x1000). For part segmentation, we report mIOU. Copy: uses the prompt’s “target” point cloud as its prediction. The **blue** and underline values indicate the best and second-best results.

Models	Venues	Reconstruction CD ↓						Denoising CD ↓						Registration CD ↓						Part Seg. mIOU↑
		L1	L2	L3	L4	L5	Avg.	L1	L2	L3	L4	L5	Avg.	L1	L2	L3	L4	L5	Avg.	
Task-specific models (trained separately)																				
PointNet [43]	CVPR’17	3.7	3.7	3.8	3.9	4.1	3.9	4.1	4.0	4.1	4.0	4.2	4.1	5.3	5.9	6.9	7.7	8.5	6.9	77.5
DGCNN [56]	TOG’19	3.9	3.9	4.0	4.1	4.3	4.0	4.7	4.5	4.6	4.5	4.7	4.6	6.2	6.7	7.3	7.4	7.7	7.1	76.1
PCT [14]	CVM’21	2.4	2.4	2.5	2.6	3.0	2.6	2.3	2.2	2.2	2.2	2.3	2.2	5.3	5.7	6.3	6.9	7.2	6.3	79.5
ACT [8]	ICLR’23	2.4	2.5	2.3	2.5	2.8	2.5	2.2	2.3	2.2	2.3	2.5	2.3	5.1	5.6	5.9	6.0	7.0	5.9	81.2
Multi-task models: share backbone + multi-task heads																				
PointNet [43]	CVPR’17	87.2	86.6	87.3	90.8	92.2	88.8	17.8	22.0	25.6	30.4	33.2	25.8	25.4	22.6	24.9	25.7	26.9	25.1	15.3
DGCNN [56]	TOG’19	38.8	36.6	37.5	37.9	42.9	37.7	6.5	6.3	6.5	6.4	7.1	6.5	12.5	14.9	17.9	19.7	20.7	17.1	17.0
PCT [14]	CVM’21	34.7	44.1	49.9	50.0	52.3	46.2	11.2	10.3	10.7	10.2	10.5	10.6	24.4	26.0	29.6	32.8	34.7	29.5	16.7
Point-MAE [42]	ECCV’22	5.5	5.5	6.1	6.4	6.4	6.0	5.6	5.4	5.6	5.5	5.8	5.6	11.4	12.8	14.8	16.0	16.9	14.5	5.4
ACT [8]	ICLR’23	7.4	6.6	6.5	6.6	7.0	6.8	7.3	6.8	7.0	6.8	7.2	7.0	12.2	14.4	19.4	25.5	29.0	20.1	12.1
I2P-MAE [71]	CVPR’23	17.0	16.0	16.7	17.2	18.5	17.2	20.6	20.4	20.1	18.3	18.8	19.6	32.5	31.3	31.1	31.6	31.2	31.5	22.6
ReCon [45]	ICML’23	12.4	12.1	12.4	12.5	13.1	12.5	20.4	24.5	27.2	29.2	32.5	26.9	14.7	16.3	19.2	21.5	22.5	18.8	7.7
In-context learning models																				
Copy		155	153	152	156	155	154	149	155	157	155	155	154	155	157	156	148	154	154	24.2
Point-BERT [68]	CVPR’22	288	285	292	286	308	292	292	293	298	296	299	296	291	295	294	295	298	294	0.7
PIC-Cat [11]	NeurIPS’23	<b>3.2</b>	<b>3.6</b>	4.6	4.9	<b>5.5</b>	<b>4.3</b>	<b>3.9</b>	<u>4.6</u>	5.3	6.0	6.8	5.3	10.0	11.4	13.8	16.9	18.6	14.1	79.0
PIC-Sep [11]	NeurIPS’23	4.7	4.3	<u>4.3</u>	<b>4.4</b>	5.7	4.7	6.3	7.2	7.9	8.2	8.6	7.6	8.6	9.2	10.2	11.3	12.4	10.3	75.0
PIC-S-Cat [31]	Arxiv’24	9.3	5.1	4.8	5.0	10.3	6.9	4.7	5.7	6.5	7.4	8.2	6.5	12.8	15.8	23.9	31.2	36.9	24.1	83.8
PIC-S-Sep [31]	Arxiv’24	4.6	4.5	4.5	4.8	7.1	5.1	9.4	11.7	12.5	13.1	13.4	12.0	6.0	<u>6.1</u>	<u>7.6</u>	<u>6.7</u>	<u>7.3</u>	<u>6.7</u>	83.7
PIC-Cat [11] + MICAS	Ours	4.6	4.2	4.5	4.8	5.7	4.7	<u>4.2</u>	<b>4.4</b>	<b>4.6</b>	<b>4.9</b>	<b>5.1</b>	<b>4.6</b>	<u>5.7</u>	6.5	9.1	12.5	15.4	9.8	<b>87.9</b>
PIC-Sep [11] + MICAS	Ours	<u>3.8</u>	<u>3.9</u>	<b>4.0</b>	<b>4.4</b>	<u>5.6</u>	<b>4.3</b>	4.4	4.9	<u>5.2</u>	<u>5.5</u>	<u>5.7</u>	<u>5.1</u>	<b>3.4</b>	<b>3.6</b>	<b>3.7</b>	<b>3.8</b>	<b>4.0</b>	<b>3.7</b>	<u>86.8</u>

“target” point patches before feeding them into the transformer, while PIC-Sep processes the “input” and “target” point patches in parallel and merges their features after several blocks. We test our method on both variants.

## 4.2. Comparisons with State-of-The-Art Methods

We compare our MICAS with various models on the ShapeNet In-Context dataset [11] in Table 1 and Figure 4.

**Comparison to Task-Specific Models.** As shown in Table 1, task-specific models set a high benchmark, delivering peak performance in reconstruction and denoising tasks due to their specialized design. However, these models require a dedicated network for each task, leading to significant complexity and resource demands. In contrast, MICAS uses only a prompt to guide a single model across multiple tasks and shows remarkable versatility, particularly excelling in registration and part segmentation. It outperforms ACT [8] by 2.2 points in registration and an impressive 6.7 points in part segmentation, showcasing its effectiveness while offering a more streamlined and efficient solution.

**Comparison to Multi-task Models.** Our proposed MICAS significantly outperforms state-of-the-art multi-task models across four tasks. Compared to Point-MAE [42], MICAS achieves better results across all five levels of datasets in the reconstruction, denoising, and registration tasks, thanks to its adaptive sampling mechanisms for task-specific feature extraction. In the part segmentation task,

MICAS achieves a remarkable mIOU of 65.3 higher than I2P-MAE [71], demonstrating its effectiveness in handling complex segmentation challenges.

**Comparison to In-context learning Models.** Within the realm of in-context learning for point clouds, two main approaches have emerged: Point-BERT [68] and PIC [11]. Therein, PIC includes two variants: \*-Cat and \*-Sep. For \*-Cat methods, although MICAS shows a minor shortfall in the reconstruction compared to PIC-Cat [42], it significantly outperforms in the denoising, registration, and part segmentation tasks. Specifically, MICAS surpasses PIC-Cat [42] by 4.3 in the registration and 8.9 in the part segmentation. Moreover, MICAS consistently outperforms PIC-S-Cat [31] across all evaluation metrics and tasks. For \*-Sep methods, MICAS achieves superior performance compared to both PIC-Sep [42] and PIC-S-Sep [31] across all metrics and tasks. In addition, qualitative results in Figure 4 further highlight the effectiveness of our proposed method.

## 4.3. Ablation Study

To demonstrate the effectiveness of MICAS, we perform an ablation study in Table 2. The results show that task-adaptive point sampling enhances denoising and part segmentation, while query-specific prompt sampling improves reconstruction and registration. They complement each other in both sampling granularity and overall performance.

**Task-adaptive Point Sampling.** We replace the farthest

Table 2. Ablation studies on the ShapeNet In-Context Dataset [11]. FPS: farthest point sampling. Point: task-adaptive point sampling. Prompt: query-specific prompt sampling. Inference time represents the average time required to process a query on three 1080ti GPUs.

ICL Model	FPS	Point	Prompt	Reconstruction CD ↓					Denoising CD ↓					Registration CD ↓					Part Seg. mIOU↑	Inference time (ms)			
				L1	L2	L3	L4	L5	Avg.	L1	L2	L3	L4	L5	Avg.	L1	L2	L3			L4	L5	Avg.
PIC-Cat [11]	✓			4.9	<b>4.1</b>	4.5	4.7	6.3	4.9	<b>4.2</b>	5.1	5.9	6.8	7.8	6.0	6.5	7.8	13.6	20.4	24.5	14.5	79.9	15.6
		✓		4.8	4.2	4.5	4.8	5.8	4.8	4.3	4.5	4.7	<b>4.9</b>	5.2	4.7	6.5	7.5	11.1	16.2	20.2	12.3	87.6	21.4
	✓		✓	4.8	<b>4.1</b>	<b>4.4</b>	<b>4.6</b>	6.2	4.8	<b>4.2</b>	5.0	5.7	6.5	7.3	5.7	<b>5.5</b>	<b>6.5</b>	10.0	14.5	17.7	10.8	80.2	44.3
		✓	✓	<b>4.6</b>	4.2	4.5	4.8	<b>5.7</b>	<b>4.7</b>	<b>4.2</b>	<b>4.4</b>	<b>4.6</b>	<b>4.9</b>	<b>5.1</b>	<b>4.6</b>	5.7	<b>6.5</b>	<b>9.1</b>	<b>12.5</b>	<b>15.4</b>	<b>9.8</b>	<b>87.9</b>	47.1
PIC-Sep [11]	✓			3.9	3.9	3.9	4.3	6.2	4.4	6.2	7.2	7.7	8.2	8.3	7.5	7.6	7.8	8.4	9.0	10.0	8.6	78.7	15.0
		✓		4.2	4.1	4.2	4.6	6.1	4.6	4.9	5.4	5.6	6.0	6.3	5.6	7.6	7.4	7.8	9.2	10.7	8.5	86.6	20.9
	✓		✓	<b>3.6</b>	<b>3.7</b>	<b>3.8</b>	<b>4.1</b>	5.8	<b>4.2</b>	5.4	6.2	6.6	7.0	7.1	6.5	<b>3.3</b>	<b>3.4</b>	<b>3.5</b>	<b>3.6</b>	<b>3.8</b>	<b>3.5</b>	79.1	44.1
		✓	✓	3.8	3.9	4.0	4.4	<b>5.6</b>	4.3	<b>4.4</b>	<b>4.9</b>	<b>5.2</b>	<b>5.5</b>	<b>5.7</b>	<b>5.1</b>	3.4	3.6	3.7	3.8	4.0	3.7	<b>86.8</b>	45.9

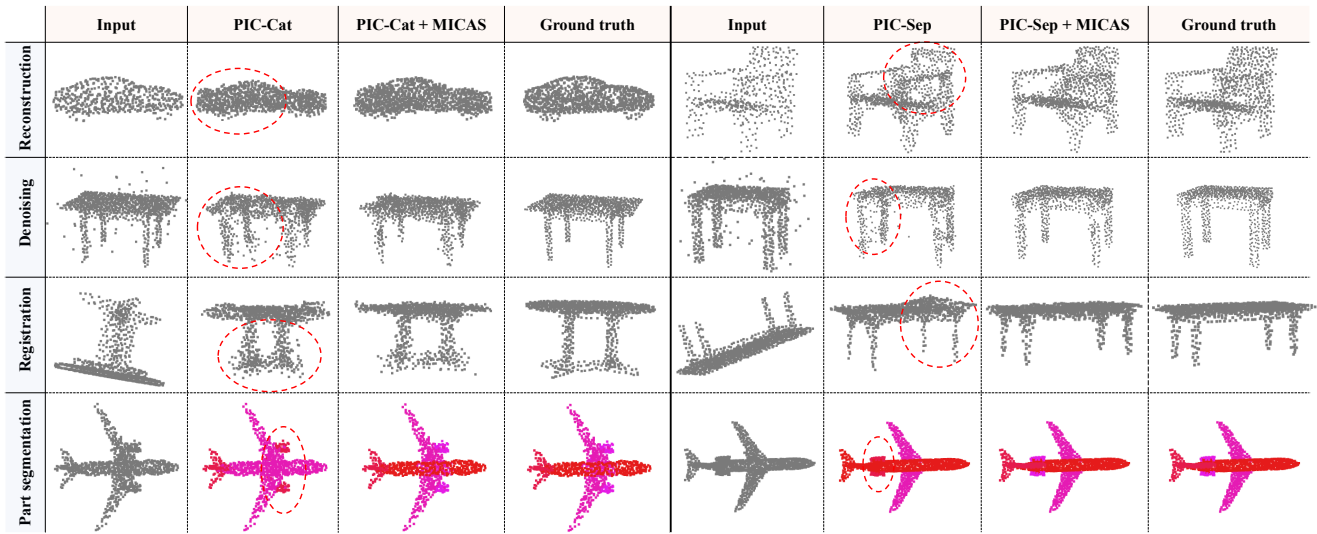


Figure 4. Qualitative experimental results compared with the PIC-Cat [11] and PIC-Sep [11]. The red ovals represent the difference between the two methods. Additional visualization results can be found in the supplementary material. (Zoom in for more details)

point sampling (FPS) used in PIC-Cat [11] and PIC-Sep [11] with task-adaptive point sampling. While task-adaptive point sampling shows both strengths and limitations compared to FPS in the reconstruction task, it demonstrates clear superiority in the denoising, registration, and part segmentation tasks. Specifically, although task-adaptive point sampling yields an average CD loss that is 0.2 higher in reconstruction compared to FPS when using PIC-Sep [11] as the ICL model, it significantly outperforms FPS across all other metrics and tasks. In addition, our proposed task-adaptive point sampling considerably enhances model performance without noticeably impacting inference speed.

**Query-specific Prompt Sampling.** We conduct two types of experiments, employing query-specific prompt sampling on FPS and task-adaptive point sampling, respectively. Our experimental results indicate that query-specific prompt sampling enhances overall performance. More importantly, the benefits of query-specific prompt sampling and task-adaptive point sampling are complementary. Specifically, task-adaptive sampling excels in enhancing

denoising and part segmentation tasks, while query-specific prompt sampling boosts performance in reconstruction and registration tasks. As shown in Table 2, combining task-adaptive point sampling with query-specific prompt sampling yields the best overall results, achieving significant performance improvements across all tasks. In addition, we find that these enhancements are achievable with only a threefold increase in inference time.

## 5. Conclusion

We undertake an early effort to address the inter-task and intra-task sensitivity issues arising from lacking context adaptation, spanning both point and prompt levels. Specifically, we propose a Multi-grained In-Context Adaptive Sampling, dubbed MICAS, which includes task-adaptive point sampling and query-specific prompt sampling. The former is engineered to interpret task information from diverse prompts and amalgamate it with the original point cloud, enabling a sampling approach that is tailored to each



prompt. The latter involves identifying the most relevant prompt for each query, which provides more effective task guidance. To our knowledge, this represents the inaugural exploration into point cloud sampling within an in-context learning framework at both point and prompt levels.

## References

- [1] Amir Bar, Yossi Gandelsman, Trevor Darrell, Amir Globerson, and Alexei Efros. Visual prompting via image inpainting. In *NeurIPS*, 2022. 1
- [2] Tolga Bolukbasi, Joseph Wang, Ofer Dekel, and Venkatesh Saligrama. Adaptive neural networks for efficient inference. In *ICML*, 2017. 6
- [3] Tom Brown, Benjamin Mann, Nick Ryder, Melanie Subbiah, Jared D Kaplan, Prafulla Dhariwal, Arvind Neelakantan, Pranav Shyam, Girish Sastry, Amanda Askell, et al. Language models are few-shot learners. In *NeurIPS*, 2020. 1
- [4] Christopher JC Burges. From ranknet to lambdarank to lambdamart: An overview. *Learning*, 2010. 6
- [5] Angel X Chang, Thomas Funkhouser, Leonidas Guibas, Pat Hanrahan, Qixing Huang, Zimo Li, Silvio Savarese, Manolis Savva, Shuran Song, Hao Su, et al. Shapenet: An information-rich 3d model repository. *arXiv*, 2015. 2, 6
- [6] Haolan Chen, Shitong Luo, Xiang Gao, and Wei Hu. Unsupervised learning of geometric sampling invariant representations for 3d point clouds. In *ICCV*, 2021. 2
- [7] Silin Cheng, Xiwu Chen, Xinwei He, Zhe Liu, and Xiang Bai. Pra-net: Point relation-aware network for 3d point cloud analysis. *IEEE Transactions on Image Processing*, 30:4436–4448, 2021. 3
- [8] Runpei Dong, Zekun Qi, Linfeng Zhang, Junbo Zhang, Jianjian Sun, Zheng Ge, Li Yi, and Kaisheng Ma. Autoencoders as cross-modal teachers: Can pretrained 2d image transformers help 3d representation learning? In *ICLR*, 2023. 7
- [9] Oren Dovrat, Itai Lang, and Shai Avidan. Learning to sample. In *CVPR*, 2019. 2, 1
- [10] Haoqiang Fan, Hao Su, and Leonidas J Guibas. A point set generation network for 3d object reconstruction from a single image. In *CVPR*, 2017. 4, 6, 7
- [11] Zhongbin Fang, Xiangtai Li, Xia Li, Joachim M Buhmann, Chen Change Loy, and Mengyuan Liu. Explore in-context learning for 3d point cloud understanding. In *NeurIPS*, 2024. 1, 2, 3, 4, 5, 6, 7, 8
- [12] Evelyn Fix. *Discriminatory analysis: nonparametric discrimination, consistency properties*. USAF school of Aviation Medicine, 1985. 4
- [13] Fabian Groh, Patrick Wieschollek, and Hendrik PA Lensch. Flex-convolution: Million-scale point-cloud learning beyond grid-worlds. In *ACCV*, 2018. 2
- [14] Meng-Hao Guo, Jun-Xiong Cai, Zheng-Ning Liu, Tai-Jiang Mu, Ralph R Martin, and Shi-Min Hu. Pct: Point cloud transformer. *Computational Visual Media*, 2021. 7
- [15] Ziyu Guo, Renrui Zhang, Xiangyang Zhu, Yiwen Tang, Xi-anzheng Ma, Jiaming Han, Kexin Chen, Peng Gao, Xi-anzhi Li, Hongsheng Li, et al. Point-bind & point-llm: Aligning point cloud with multi-modality for 3d understanding, generation, and instruction following. *arXiv preprint arXiv:2309.00615*, 2023. 3
- [16] Shuting He, Henghui Ding, Xudong Jiang, and Bihan Wen. Segpoint: Segment any point cloud via large language model. In *ECCV*, 2025. 3
- [17] Qingyong Hu, Bo Yang, Linhai Xie, Stefano Rosa, Yulan Guo, Zhihua Wang, Niki Trigoni, and Andrew Markham. Randla-net: Efficient semantic segmentation of large-scale point clouds. In *CVPR*, 2020. 2
- [18] Zhangjin Huang, Yuxin Wen, Zihao Wang, Jinjuan Ren, and Kui Jia. Surface reconstruction from point clouds: A survey and a benchmark. *IEEE Transactions on Pattern Analysis and Machine Intelligence*, 2024. 1
- [19] Eric Jang, Shixiang Gu, and Ben Poole. Categorical reparameterization with gumbel-softmax. In *ICLR*, 2016. 2, 4, 5
- [20] Alireza Javaheri, Catarina Brites, Fernando Pereira, and João Ascenso. Subjective and objective quality evaluation of 3d point cloud denoising algorithms. In *ICMEW*, 2017. 3
- [21] Philipp Jenke, Michael Wand, Martin Bokeloh, Andreas Schilling, and Wolfgang Straßer. Bayesian point cloud reconstruction. In *Computer graphics forum*, 2006. 3
- [22] Jincen Jiang, Qianyu Zhou, Yuhang Li, Xuequan Lu, Meili Wang, Lizhuang Ma, Jian Chang, and Jian Jun Zhang. Dg-pic: Domain generalized point-in-context learning for point cloud understanding. In *ECCV*, 2025. 1, 3
- [23] Jeesoo Kim, Junsuk Choe, Sangdoon Yun, and Nojun Kwak. Normalization matters in weakly supervised object localization. In *ICCV*, 2021. 6
- [24] Maxim Kolodiazhnyi, Anna Vorontsova, Anton Konushin, and Danila Rukhovich. Oneformer3d: One transformer for unified point cloud segmentation. In *CVPR*, 2024. 1
- [25] Loic Landrieu and Martin Simonovsky. Large-scale point cloud semantic segmentation with superpoint graphs. In *CVPR*, 2018. 4
- [26] Itai Lang, Asaf Manor, and Shai Avidan. Samplenet: Differentiable point cloud sampling. In *CVPR*, 2020. 2, 3, 1
- [27] Itay Levy, Ben Bogin, and Jonathan Berant. Diverse demonstrations improve in-context compositional generalization. In *ACL*, 2023. 3
- [28] Xiaonan Li, Kai Lv, Hang Yan, Tianyang Lin, Wei Zhu, Yuan Ni, Guotong Xie, Xiaoling Wang, and Xipeng Qiu. Unified demonstration retriever for in-context learning. In *ACL*, 2023. 3, 5, 6
- [29] Yangyan Li, Rui Bu, Mingchao Sun, Wei Wu, Xinhan Di, and Baoquan Chen. Pointcnn: Convolution on x-transformed points. In *NeurIPS*, 2018. 2
- [30] Jiachang Liu, Dinghan Shen, Yizhe Zhang, Bill Dolan, Lawrence Carin, and Weizhu Chen. What makes good in-context examples for gpt-3? In *DeeLIO*, 2022. 3
- [31] Mengyuan Liu, Zhongbin Fang, Xia Li, Joachim M Buhmann, Xiangtai Li, and Chen Change Loy. Point-in-context: Understanding point cloud via in-context learning. *arXiv*, 2024. 1, 4, 7
- [32] Yongcheng Liu, Bin Fan, Shiming Xiang, and Chunhong Pan. Relation-shape convolutional neural network for point cloud analysis. In *CVPR*, 2019. 2

- [33] Ilya Loshchilov and Frank Hutter. Sgdr: Stochastic gradient descent with warm restarts. In *ICLR*, 2017. 6
- [34] Shitong Luo and Wei Hu. Score-based point cloud denoising. In *ICCV*, 2021. 1, 3
- [35] Yawei Luo and Yi Yang. Large language model and domain-specific model collaboration for smart education. *Frontiers of Information Technology & Electronic Engineering*, 25(3): 333–341, 2024. 1
- [36] Xu Ma, Can Qin, Haoxuan You, Haoxi Ran, and Yun Fu. Re-thinking network design and local geometry in point cloud: A simple residual mlp framework. In *ICLR*, 2022. 2
- [37] Priyanka Mandikal and Venkatesh Babu Radhakrishnan. Dense 3d point cloud reconstruction using a deep pyramid network. In *WACV*, 2019. 1, 3
- [38] Amit Moryossef, Yoav Goldberg, and Ido Dagan. Step-by-step: Separating planning from realization in neural data-to-text generation. *arXiv preprint arXiv:1904.03396*, 2019. 6
- [39] Ehsan Nezhadarya, Ehsan Taghavi, Ryan Razani, Bingbing Liu, and Jun Luo. Adaptive hierarchical down-sampling for point cloud classification. In *CVPR*, 2020. 3
- [40] Alex Nichol, Heewoo Jun, Prafulla Dhariwal, Pamela Mishkin, and Mark Chen. Point-e: A system for generating 3d point clouds from complex prompts. *arXiv preprint arXiv:2212.08751*, 2022. 3
- [41] Ercong Nie, Sheng Liang, Helmut Schmid, and Hinrich Schütze. Cross-lingual retrieval augmented prompt for low-resource languages. In *ACL*, 2023. 3
- [42] Yatian Pang, Wenxiao Wang, Francis EH Tay, Wei Liu, Yonghong Tian, and Li Yuan. Masked autoencoders for point cloud self-supervised learning. In *ECCV*, 2022. 7
- [43] Charles R Qi, Hao Su, Kaichun Mo, and Leonidas J Guibas. Pointnet: Deep learning on point sets for 3d classification and segmentation. In *CVPR*, 2017. 4, 6, 7, 1, 2
- [44] Charles Ruizhongtai Qi, Li Yi, Hao Su, and Leonidas J Guibas. Pointnet++: Deep hierarchical feature learning on point sets in a metric space. In *NeurIPS*, 2017. 2, 4
- [45] Zekun Qi, Runpei Dong, Guofan Fan, Zheng Ge, Xiangyu Zhang, Kaisheng Ma, and Li Yi. Contrast with reconstruct: Contrastive 3d representation learning guided by generative pretraining. In *ICML*, 2023. 7
- [46] Alec Radford, Jong Wook Kim, Chris Hallacy, Aditya Ramesh, Gabriel Goh, Sandhini Agarwal, Girish Sastry, Amanda Askell, Pamela Mishkin, Jack Clark, et al. Learning transferable visual models from natural language supervision. In *ICML*, 2021. 3
- [47] Ohad Rubin, Jonathan Herzig, and Jonathan Berant. Learning to retrieve prompts for in-context learning. In *NAACL*, 2022. 3
- [48] Ziyu Shan, Qi Yang, Rui Ye, Yujie Zhang, Yiling Xu, Xiaozhong Xu, and Shan Liu. Gpa-net: No-reference point cloud quality assessment with multi-task graph convolutional network. *TVCG*, 2023. 1
- [49] Feifei Shao, Yawei Luo, Ping Liu, Jie Chen, Yi Yang, Yulei Lu, and Jun Xiao. Active learning for point cloud semantic segmentation via spatial-structural diversity reasoning. In *ACM MM*, 2022. 1, 4
- [50] Yuan Tang, Xu Han, Xianzhi Li, Qiao Yu, Yixue Hao, Long Hu, and Min Chen. Minigpt-3d: Efficiently aligning 3d point clouds with large language models using 2d priors. In *ACM MM*, 2024. 3
- [51] Hugues Thomas, Charles R Qi, Jean-Emmanuel Deschaud, Beatriz Marcotequi, François Goulette, and Leonidas J Guibas. Kpconv: Flexible and deformable convolution for point clouds. In *ICCV*, 2019. 2
- [52] Hugo Touvron, Thibaut Lavril, Gautier Izacard, Xavier Martinet, Marie-Anne Lachaux, Timothée Lacroix, Baptiste Rozière, Naman Goyal, Eric Hambro, Faisal Azhar, et al. Llama: Open and efficient foundation language models. *arXiv preprint arXiv:2302.13971*, 2023. 3
- [53] Nazanin Vafaei, Rita A Ribeiro, and Luis M Camarinha-Matos. Assessing normalization techniques for simple additive weighting method. *Procedia Computer Science*, 199: 1229–1236, 2022. 6
- [54] Xinlong Wang, Wen Wang, Yue Cao, Chunhua Shen, and Tiejun Huang. Images speak in images: A generalist painter for in-context visual learning. In *CVPR*, 2023. 1
- [55] Xinlong Wang, Xiaosong Zhang, Yue Cao, Wen Wang, Chunhua Shen, and Tiejun Huang. Seggpt: Segmenting everything in context. In *ICCV*, 2023. 1
- [56] Yue Wang, Yongbin Sun, Ziwei Liu, Sanjay E Sarma, Michael M Bronstein, and Justin M Solomon. Dynamic graph cnn for learning on point clouds. *ToG*, 2019. 7, 1, 2
- [57] Zeyong Wei, Honghua Chen, Liangliang Nan, Jun Wang, Jing Qin, and Mingqiang Wei. Pathnet: Path-selective point cloud denoising. *IEEE Transactions on Pattern Analysis and Machine Intelligence*, 2024. 1
- [58] Cheng Wen, Baosheng Yu, and Dacheng Tao. Learnable skeleton-aware 3d point cloud sampling. In *CVPR*, 2023. 2, 3, 5, 1
- [59] Chengzhi Wu, Junwei Zheng, Julius Pfommer, and Jürgen Beyerer. Attention-based point cloud edge sampling. In *CVPR*, 2023. 3
- [60] Zhenyu Wu, Kun Li, Yuhu Wu, Xin Zhang, and Shengming Li. Indexsample: A learnable sampling network in point cloud classification. In *SICE*, 2021. 3
- [61] Runsen Xu, Xiaolong Wang, Tai Wang, Yilun Chen, Jiangmiao Pang, and Dahua Lin. Pointllm: Empowering large language models to understand point clouds. In *ECCV*, 2025. 3
- [62] Xin Xu, Yue Liu, Panupong Pasupat, Mehran Kazemi, et al. In-context learning with retrieved demonstrations for language models: A survey. *arXiv*, 2024. 1, 3, 6
- [63] Xu Yan, Chaoda Zheng, Zhen Li, Sheng Wang, and Shuguang Cui. Pointasnl: Robust point clouds processing using nonlocal neural networks with adaptive sampling. In *CVPR*, 2020. 2, 3, 1
- [64] Heng Yang, Jingnan Shi, and Luca Carlone. Teaser: Fast and certifiable point cloud registration. *IEEE Transactions on Robotics*, 2020. 1, 4
- [65] Jiancheng Yang, Qiang Zhang, Bingbing Ni, Linguo Li, Jinxian Liu, Mengdie Zhou, and Qi Tian. Modeling point clouds with self-attention and gumbel subset sampling. In *CVPR*, 2019. 3, 4, 5

- [66] Li Yi, Vladimir G Kim, Duygu Ceylan, I-Chao Shen, Mengyan Yan, Hao Su, Cewu Lu, Qixing Huang, Alla Sheffer, and Leonidas Guibas. A scalable active framework for region annotation in 3d shape collections. *ToG*, 2016. 2, 6
- [67] Wenhao Yu, Dan Iter, Shuohang Wang, Yichong Xu, Mingxuan Ju, Soumya Sanyal, Chenguang Zhu, Michael Zeng, and Meng Jiang. Generate rather than retrieve: Large language models are strong context generators. In *ICLR*, 2023. 3
- [68] Xumin Yu, Lulu Tang, Yongming Rao, Tiejun Huang, Jie Zhou, and Jiwen Lu. Point-bert: Pre-training 3d point cloud transformers with masked point modeling. In *CVPR*, 2022. 7
- [69] Yihan Zeng, Chenhan Jiang, Jiageng Mao, Jianhua Han, Chaoqiang Ye, Qingqiu Huang, Dit-Yan Yeung, Zhen Yang, Xiaodan Liang, and Hang Xu. Clip2: Contrastive language-image-point pretraining from real-world point cloud data. In *CVPR*, 2023. 3
- [70] Renrui Zhang, Ziyu Guo, Wei Zhang, Kunchang Li, Xupeng Miao, Bin Cui, Yu Qiao, Peng Gao, and Hongsheng Li. Pointclip: Point cloud understanding by clip. In *Proceedings of the IEEE/CVF conference on computer vision and pattern recognition*, pages 8552–8562, 2022. 3
- [71] Renrui Zhang, Lihui Wang, Yu Qiao, Peng Gao, and Hongsheng Li. Learning 3d representations from 2d pre-trained models via image-to-point masked autoencoders. In *CVPR*, 2023. 7
- [72] Yu Zhang and Qiang Yang. A survey on multi-task learning. *TKDE*, 2021. 1
- [73] Yaojie Zhang, Weijun Wang, Tianlun Huang, Zhiyong Wang, and Wei Feng. Svc: Sight view constraint for robust point cloud registration. *Image and Vision Computing*, page 105315, 2024. 1
- [74] Zhuosheng Zhang, Aston Zhang, Mu Li, and Alex Smola. Automatic chain of thought prompting in large language models. In *ICLR*, 2023. 3
- [75] Luda Zhao, Yihua Hu, Xing Yang, Zhenglei Dou, and Linshuang Kang. Robust multi-task learning network for complex lidar point cloud data preprocessing. *Expert Systems with Applications*, 2024. 1



# MICAS: Multi-grained In-Context Adaptive Sampling for 3D Point Cloud Processing

## Supplementary Material

### Summary of the Appendix

To complement the main paper, this supplementary material provides additional details and insights, structured as follows:

- Sec. 6 presents an additional ablation study to demonstrate the robustness of our proposed MICAS.
- Sec. 7 provides further qualitative analysis by showcasing sampled points.
- Sec. 8 discusses the limitations of our approach and its broader impacts.

### 6. Ablation Study: Robustness Analysis

In the task-adaptive point sampling module and query-specific prompt sampling module of our proposed MICAS, we design the task encoder, point encoder, and prompt sampling module based on PointNet [43]. To evaluate the robustness of MICAS, we conduct an additional ablation experiment by replacing PointNet with DGCNN [56], a model widely used for CNN-based high-level tasks on point clouds, such as classification and segmentation. Unlike PointNet [43], which relies on a multilayer perceptron (MLP) architecture, DGCNN [56] employs a dynamic graph CNN framework and introduces the EdgeConv operation. This operation effectively captures local geometric features of point clouds while maintaining permutation invariance.

The experimental results presented in Table A1, show that the performance trend of MICAS remains consistent across in-context learning models, including PIC-Cat [11] and PIC-Sep [11], regardless of whether PointNet [43] or DGCNN [56] is used. These findings highlight the robustness of MICAS, demonstrating its reliability across different in-context learning frameworks and point cloud models.

### 7. More Qualitative Analysis

To demonstrate the effectiveness of our proposed MICAS in central point sampling and prediction, we present a visual comparison between our task-adaptive point sampling method and Farthest Point Sampling (FPS) used in PIC-Cat [11] and PIC-Sep [11]. As shown in Figures A1 and A2, our proposed MICAS consistently selects higher-quality central points, delivering superior outcomes and overcoming the limitations of FPS. For instance, in the denoising task, FPS often prioritizes outliers, frequently selecting noisy points as central points. In contrast, MICAS effec-

tively avoids these noisy points, focusing on more meaningful and valuable selections. In the reconstruction and registration tasks, MICAS outperforms PIC-Cat [11] and PIC-Sep [11] by producing target point clouds with clearer contours and more accurate shapes. Similarly, in the part segmentation task, MICAS achieves accurate segmentation even in areas where PIC-Cat [11] and PIC-Sep [11] encounter segmentation errors. These visualization results underscore the significance and effectiveness of our proposed MICAS in advancing point cloud in-context learning.

### 8. Discussion

#### 8.1. Limitations

While our proposed MICAS represents a pioneering effort to address inter-task and intra-task sensitivity challenges in point cloud in-context learning, it has a limitation. Specifically, in the query-specific prompt sampling, we prioritize selecting the “best-performing” prompt from a sampled set of 8 candidate prompts. This process requires predicting the sampling probability for each of the 8 candidate prompts, which increases the model’s inference time. As shown in Table 2 of the main paper, the query-specific prompt sampling introduces additional computation, adding approximately 25 ms to the inference time. Nonetheless, despite this slight increase in inference time, the query-specific prompt sampling achieves significant performance gains, particularly in the registration task.

In future work, we recommend addressing this limitation by making the prompt sampling module more lightweight and reducing the size of the prompt candidate pool. Specifically, a simplified prompt sampling module could be developed to streamline the prediction of sampling probabilities and enhance prediction speed. Furthermore, reducing the number of candidate prompts from 8 to 4 or even 2 would significantly lower the computational burden, thereby reducing the overall inference time.

#### 8.2. Broader Impacts

This work highlights the limitations of existing learnable task-based sampling approaches [9, 26, 58, 63], which focus solely on inter-point cloud adaptive sampling within the same task and lack the capability to perform inter-task adaptive sampling within the same point cloud. To address this gap, we propose a novel Multi-grained In-Context Adaptive Sampling mechanism, referred to as MICAS, which

Table A1. Robustness studies on the ShapeNet In-Context Dataset [11]. ICL Model: in-context learning model. FPS: farthest point sampling. Point: task-adaptive point sampling. Prompt: query-specific prompt sampling. Introduced Model: the network model used by the task encoder, point encoder, and prompt sampling module in our proposed MICAS.

ICL Model	FPS	Point	Prompt	Reconstruction CD ↓						Denosing CD ↓						Registration CD ↓						Part Seg. mIOU↑	Introduced Model
				L1	L2	L3	L4	L5	Avg.	L1	L2	L3	L4	L5	Avg.	L1	L2	L3	L4	L5	Avg.		
PIC-Cat [11]	✓	✓	✓	4.9	<b>4.1</b>	<b>4.5</b>	<b>4.7</b>	6.3	4.9	<b>4.2</b>	5.1	5.9	6.8	7.8	6.0	6.5	7.8	13.6	20.4	24.5	14.5	79.9	-
				4.8	4.2	<b>4.5</b>	4.8	5.8	4.8	4.3	4.5	4.7	<b>4.9</b>	5.2	4.7	6.5	7.5	11.1	16.2	20.2	12.3	87.6	PointNet [43]
				<b>4.6</b>	4.2	<b>4.5</b>	4.8	<b>5.7</b>	<b>4.7</b>	<b>4.2</b>	<b>4.4</b>	<b>4.6</b>	<b>4.9</b>	<b>5.1</b>	<b>4.6</b>	<b>5.7</b>	<b>6.5</b>	<b>9.1</b>	<b>12.5</b>	<b>15.4</b>	<b>9.8</b>	<b>87.9</b>	PointNet [43]
	✓	✓	✓	4.9	<b>4.1</b>	<b>4.5</b>	<b>4.7</b>	6.3	<b>4.9</b>	4.2	5.1	5.9	6.8	7.8	6.0	6.5	7.8	13.6	20.4	24.5	14.5	79.9	-
				4.9	4.2	4.6	4.9	5.9	<b>4.9</b>	4.1	4.3	4.6	<b>4.8</b>	5.0	4.6	6.6	7.5	11.5	16.7	20.5	12.6	<b>85.5</b>	DGCNN [56]
				<b>4.8</b>	4.2	4.6	4.9	<b>5.8</b>	<b>4.9</b>	<b>4.0</b>	<b>4.3</b>	<b>4.5</b>	<b>4.8</b>	<b>4.9</b>	<b>4.5</b>	<b>5.8</b>	<b>6.7</b>	<b>9.5</b>	<b>13.0</b>	<b>15.9</b>	<b>10.2</b>	85.4	DGCNN [56]
PIC-Sep [11]	✓	✓	✓	3.9	<b>3.9</b>	<b>3.9</b>	<b>4.3</b>	6.2	4.4	6.2	7.2	7.7	8.2	8.3	7.5	7.6	7.8	8.4	9.0	10.0	8.6	78.7	-
				4.2	4.1	4.2	4.6	6.1	4.6	4.9	5.4	5.6	6.0	6.3	5.6	7.6	7.4	7.8	9.2	10.7	8.5	86.6	PointNet [43]
				<b>3.8</b>	<b>3.9</b>	4.0	4.4	<b>5.6</b>	<b>4.3</b>	<b>4.4</b>	<b>4.9</b>	<b>5.2</b>	<b>5.5</b>	<b>5.7</b>	<b>5.1</b>	<b>3.4</b>	<b>3.6</b>	<b>3.7</b>	<b>3.8</b>	<b>4.0</b>	<b>3.7</b>	<b>86.8</b>	PointNet [43]
	✓	✓	✓	<b>3.9</b>	<b>3.9</b>	<b>3.9</b>	<b>4.3</b>	<b>6.2</b>	<b>4.4</b>	6.2	7.2	7.7	8.2	8.3	7.5	7.6	7.8	8.4	9.0	10.0	8.6	78.7	-
				4.4	4.2	4.3	4.9	6.7	4.9	4.9	5.4	5.7	6.0	6.3	5.7	8.0	8.0	8.6	9.3	9.8	8.7	83.9	DGCNN [56]
				4.0	4.0	4.2	4.6	<b>6.2</b>	4.6	<b>4.3</b>	<b>4.8</b>	<b>5.1</b>	<b>5.5</b>	<b>5.8</b>	<b>5.1</b>	<b>3.6</b>	<b>3.8</b>	<b>3.8</b>	<b>3.9</b>	<b>4.1</b>	<b>3.9</b>	<b>84.0</b>	DGCNN [56]

enables adaptive sampling within the same point cloud by leveraging various prompts.

In summary, our work represents the first shift in point cloud sampling from inter-point cloud adaptive sampling within the same task to inter-task adaptive sampling within the same point cloud. Furthermore, the proposed MICAS contributes positively to the research community by advancing the field of point cloud processing and inspiring future innovations in adaptive in-context learning frameworks.

	Input	PIC-Cat sampling points	PIC-Cat prediction	PIC-Cat + MICAS sampling points	PIC-Cat + MICAS prediction	Ground truth
Reconstruction						
Denoising						
Registration						
Part segmentation						

Figure A1. Qualitative experimental results compared with the PIC-Cat [11]. The red and green points denote the central points selected by PIC-Cat and our proposed MICAS, respectively. (Zoom in for more details)

	Input	PIC-Sep sampling points	PIC-Sep prediction	PIC-Sep + MICAS sampling points	PIC-Sep + MICAS prediction	Ground truth
Reconstruction						
Denoising						
Registration						
Part segmentation						

Figure A2. Qualitative experimental results compared with the PIC-Sep [11]. The red and green points denote the central points selected by PIC-Sep and our proposed MICAS, respectively. (Zoom in for more details)